Journal of
Mechanics of
Materials and Structures

INTEGRATED MODELLING OF TOOL WEAR AND MICROSTRUCTURAL EVOLUTION INTERNAL RELATIONS IN FRICTION STIR WELDING WITH WORN PIN PROFILES

Zhao Zhang and Zhijun Tan

Volume 14, No. 4 July 2019

msp

JOURNAL OF MECHANICS OF MATERIALS AND STRUCTURES
Vol. 14, No. 4, 2019
dx.doi.org/10.2140/jomms.2019.14.537

INTEGRATED MODELLING OF TOOL WEAR AND MICROSTRUCTURAL EVOLUTION INTERNAL RELATIONS IN FRICTION STIR WELDING WITH WORN PIN PROFILES

ZHAO ZHANG AND ZHIJUN TAN

An adaptive remeshing model was coupled with the Archard equation to calculate the tool wear in friction stir welding (FSW). The Monte Carlo method was used to simulate recrystallization in FSW with worn tools. In addition, experiments were used to validate the predicted temperatures and microstructures. As indicated by the results, appropriate tool wear can lead to self-optimization of the tool in FSW. This wear mechanism is controlled by the change in the average strain rate during the FSW process. The average strain rate first increases and then decreases with tool wear, which is the key factor when determining the final grains. An appropriate amount of tool wear can lead to smaller grains in the stirring zone of FSW whereas excess tool wear can lead to larger grains.

1. Introduction

Friction stir welding (FSW) has emerged in recent decades and has quickly been applied in various industries due to its advantages, including no melting, no pollution, and low residual distortions. Furthermore, FSW is suitable for light alloys, such as aluminum and magnesium alloys. Optimization of the process parameters can lead to high-quality friction stir welds without defects [Yang et al. 2018; He et al. 2017; Zhang and Zhang 2007; Ebrahimpour et al. 2019].

In FSW, the tool plays the key role for the final weld quality. De et al. [2014] tested the durability of a FSW welding tool of mild steel and found that the higher temperature, caused by increasing the tool rotation speed or the tool diameter, can lead to an increase of the tool durability. Sahlot et al. [2018] studied the tool wear in FSW of the CuCrZr alloy and found that the pin profile changes due to wear, resulting in root defects for a long weld distance. Suresha et al. [2011] studied the tool profile effects on the tensile properties of friction stir welded AA7075-T6. Moreover, Chen and Nakata [2009] studied the effect of tool geometry on microstructural changes as well as the mechanical properties in friction stir lap welding. Mehta et al. [2011] studied the influence of tool geometry in FSW and optimized the tool shoulder diameter. Zhang and Wu [2015] studied the tool diameter effect in FSW and correlated the changes of strain rates and temperatures with the grain sizes. The tool size effect on the grains was also studied by Zhang et al. [2014], as well as the effect on temperatures and material deformations [Zhang et al. 2009]. Mastanaiah et al. [2018] investigated the role of a hybrid tool pin profile compared with the conventional pin profile. Shindo et al. [2002] and Prado et al. [2003] found that there is self-optimization for tool wear in FSW. The wear rate decreases with the increase of the tool wear in FSW.

Sahlot and Arora [2018] established a numerical model based on Modified Archard's wear equation to investigate the tool wear in FSW with experimental validations, finding that the wear amount is more

Keywords: friction stir welding, wear, Monte Carlo.

obvious near the pin tip. The wear is more at the beginning and becomes less at long traverse. Tool wear can lead to the changes of pin profiles in FSW. In turn, the change in the pin profile can lead to a change in material flow, as indicated by Beygi et al. [2018], affecting the microstructures in welding zones. The relationship between microstructure and tool wear is very important when conducting a detailed investigation of the FSW mechanism.

The microstructural evolution can also be altered owning to the profile changes caused by tool wear. A numerical scheme for the microstructures provides an insight into the FSW process. Meanwhile, the recrystallization and grain growth in the stirring zone (SZ) and the grain coarsening in the heat-affected zone are usually simulated by a Monte Carlo method and cellular automaton method, respectively. Zhang et al. [2016] proposed a Monte Carlo method to simulate the microstructural changes in FSW, then further considered the effect of precipitate, as indicated in [Wu and Zhang 2017]. The evolution of the precipitates was determined by a numerical model, as displayed in [Zhang et al. 2017]. The Monte Carlo method was further extended to a 3D case in [Zhang and Hu 2018]. Another method to predict the grain sizes in FSW is cellular automaton. Earlier work for cellular automata coupled with a finite element method (FEM) was conducted by Saluja et al. [2012], then Song et al. [2014] to predict the grain sizes in FSW. Akbari et al. [2016] established a cellular automaton model to predict the grain sizes in the FSW of a magnesium alloy. Meanwhile, Valvi et al. [2016] combined the cellular automata method and a FEM to predict the grain sizes in the FSW of aluminum alloys.

Although the tool wear is not serious in the FSW of AA6061, there is evidence to show that it can be found for long-term use, i.e., for the FSW of AA6061. Thus, it is interesting to study how the worn tool affects the key phenomena, including the temperatures and recrystallizations in FSW. To understand the mechanism of tool wear and the wear-induced self-optimization in FSW, it is important to conduct theoretical and numerical analyses on the internal relationships among the internal parameters. Experiments must be used to validate the numerical models, then the internal relationships between the tool wear and microstructures can be established. In the current work, tool wear was calculated with validation from literatures. A Monte Carlo method was used to simulate the grain evolutions in the SZ. In addition, an experiment was performed to validate the grain sizes. Then, the correlation between the tool wear and the microstructures could be established. The systematic work was used for the investigation on the self-optimization mechanism of the tool in FSW.

2. Experimental procedure

The FSW machine and the instruments used in the experiment are shown in Figure 1. AA6061-T6 was selected as the welding material. The rotating speed was 1000 rpm and the transverse speed was 1 mm/s. The tool material was H13 steel. In addition, a scanning electron microscope (SEM) system was used to validate the grain morphologies and sizes predicted by the Monte Carlo method with a worn tool. An infrared radiation thermometer was used to validate the predicted temperature field.

A microstructure analysis was performed on the cross-section of the weld by field-emission scanning electron microscopy (FE-SEM, Supra-55, Carl Zeiss Sigma NTS Gmbh, Germany). The SEM samples were ground and polished with a diamond paste of 0.5 μm. To investigate the grain size distribution of the weld zone, the samples were etched in the Keller's reagent for 200 s. The average grain size was then calculated using the linear intercept method: $d = 1.56L$, where L is the intercept length.

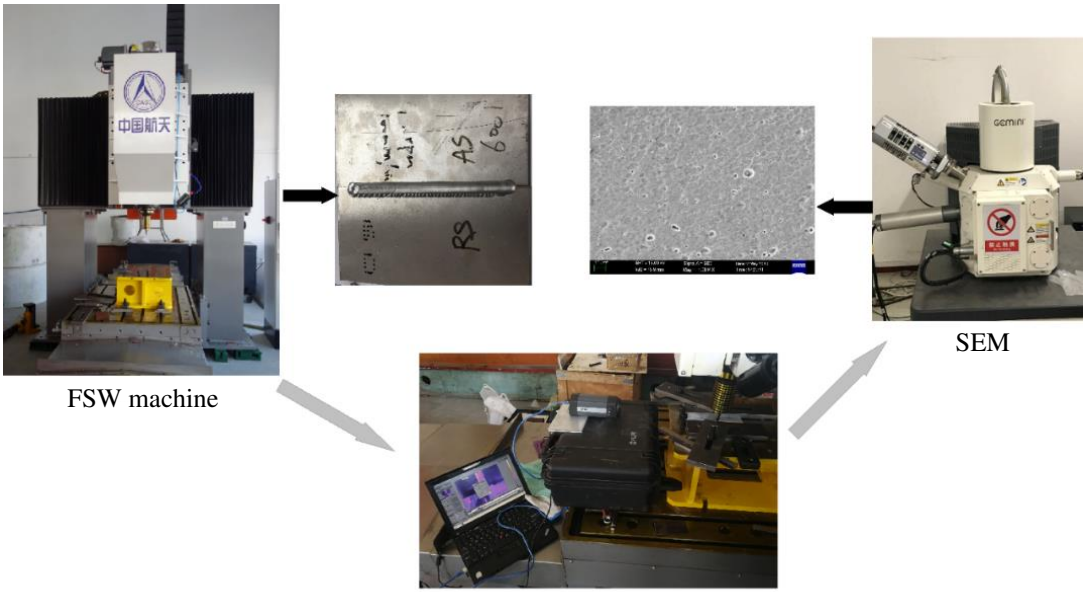

Figure 1. FSW machine and the used instruments.

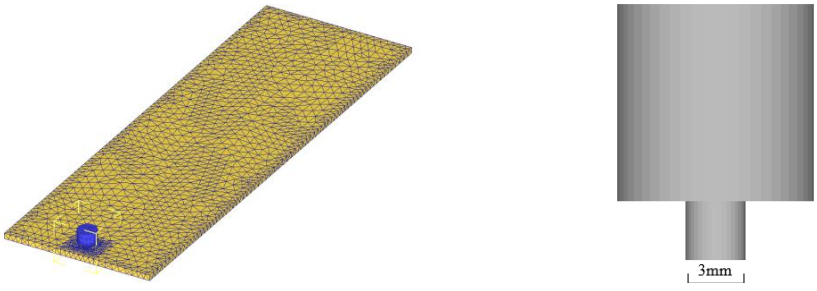

Figure 2. FSW model and welding tool before wear: FEM model (left) and welding tool (right).

3. Numerical models

An adaptive remeshing model was used to simulate the FSW process based on DEFORM^{3D}, as shown in Figure 2 (left). The initial mesh sizes ranged from 2 mm–5.4 mm. Then, the mesh sizes ranged from 0.4 mm–1 mm in the remeshing region in the SZ. The used initial tool before wear is shown in Figure 2 (right). The shoulder diameter is 10 mm and the pin diameter is 3 mm. The pin is slightly shorter than the thickness of the welding plate, which is of the same length as that used in the experiment. The rotating speed was 1000 rpm while the transverse speed was 1 mm/s.

The shear friction model was used for the contact behaviors on the tool-plate interface:

$$\tau = mk, \tag{1}$$

where k is the yield shear stress and m is the frictional factor, which is selected as 0.6 according to [Wan et al. 2016].

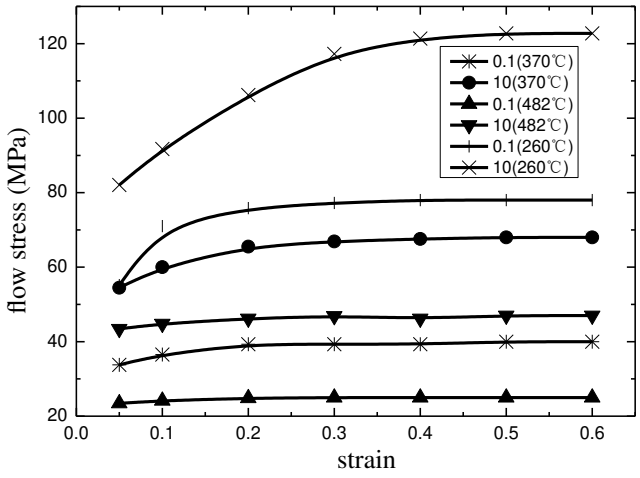

Figure 3. Mechanical properties of AA6061-T6.

The yield shear stress can be determined by the shear failure criteria:

$$k = \sigma_s/\sqrt{3}, \tag{2}$$

where σ_s is the yield strength. The tabulated flow stress was used as functions of the strain rates and temperatures:

$$\sigma_y = \sigma_y(\bar{\varepsilon}^p, \dot{\bar{\varepsilon}}^p, T), \tag{3}$$

where $\bar{\varepsilon}^p$ is the equivalent plastic strain and $\dot{\bar{\varepsilon}}^p$ is the equivalent plastic strain rate.

The relations between the flow stresses and the strain rates and temperatures are shown in Figure 3 (data from DEFORM^{3D}). Heat is generated by both friction and plastic deformation, with friction being the main contributor. A detailed description on the adaptive remeshing model can be found in [Zhang and Wan 2012].

The Archard equation was used to calculate the tool wear in FSW [Lee and Jou 2003]:

$$W = \int K \frac{p^a \cdot v^b}{H^c}\, dt, \tag{4}$$

where W is the total wear depth of the tool, p is the pressure on the welding tool, v is the sliding velocity, and H is the hardness of the welding tool, taken as 62HRC. Additionally, $K = 2 \cdot 10^{-5}$ for AA6061+20%Al_2O_3 and $K = 2 \cdot 10^{-8}$ for AA6061-T6; a and b are commonly taken as 1, and $c = 1.75$ for the welding tool.

The simulation was divided into two steps. In the first step, the FSW process was simulated in DEFORM^{3D}. The obtained data was combined with the Archard equation to simulate the tool wear. In the following step, the worn tools obtained at different instances were used in numerical models to connect the worn shapes with the FSW temperature histories. The obtained temperatures were then combined with the developed Monte Carlo method to correlate the tool wear with the microstructural evolutions in FSW with worn pin profiles.

physical property	value
average number per unit area (Z)	$4.31 \cdot 10^{20}$ atom/m^2
Planck constant (h)	$6.624 \cdot 10^{-34}$ J s
accommodation probability (A)	1
Avogadro's number (N_a)	$6.02 \cdot 10^{23}$ mol^{-1}
atom molar volume (V_m)	$1.0 \cdot 10^{-5}$ m^3/mol
fusion entropy (ΔS_f)	11.5
activation enthalpy (Q)	156 kJ/mol
boundary energy (γ)	0.5 J/m^2
gas constant (R)	8.31 J mol^{-1} K^{-1}
DRX constant (N_0)	10^{24} m^{-3}

Table 1. Material parameters.

A Monte Carlo method was used to simulate the recrystallization and the following grain growth in FSW. In the previous work by Zhang et al. [2016], a relation between the Monte Carlo step and the real temperature was established as

$$(MCS)^{(n+1)n_1} = \left(\frac{L_0}{K_1 l}\right)^{n+1} + \frac{(n+1)\,\alpha C_1^n}{(K_1 l)^{n+1}} \sum \left[\exp^n\left(-\frac{Q}{RT_i}\right) t_i\right], \tag{5}$$

where C_1 can be described by

$$C_1 = \frac{2A\gamma Z V_m^2}{N_a^2 h} \exp\left(\frac{\Delta S_f}{R}\right), \tag{6}$$

where A, Z, V_m, ΔS_f, R, N_a, γ, Q, and h are summarized in Table 1. A detailed description on the Monte Carlo method can be found in [Zhang et al. 2016].

The nucleation rate is a function of the strain rate $\dot{\bar{\varepsilon}}$ [Grujicic et al. 2015]:

$$\dot{n} = N_0\, \dot{\bar{\varepsilon}} \exp(-Q/RT), \tag{7}$$

where N_0 is a constant and $\dot{\bar{\varepsilon}}$ is the equivalent strain rate in the SZ, which is obtained using the FEM.

4. Results and discussion

To validate the tool wear predictions, AA6061+20%Al_2O_3 was used. The tool wear rate decreased with the increase of the wear depth. Furthermore, the numerical model fitted well with the experimental observation by Prado et al. [2003], as shown in Figure 4 (left). When AA6061-T6 was used, the tool wear obviously decreased. For the short welding distance for the FSW of AA6061-T6, the tool wear is difficult to observe. This phenomenon was also noticed in the experiment by Prado et al. [2001]. In comparison with the experiments, the current model on tool wear can be validated.

Figure 4 (right) shows the variation of the wear depth with the welding distance in the FSW of AA6061-T6. With the increase of the wear depth, the wear rate becomes smaller. This indicates a self-optimization for the welding tool in FSW. The wear mainly occurs near the tip of the welding pin. However, the material near the root of the pin is hardly worn.

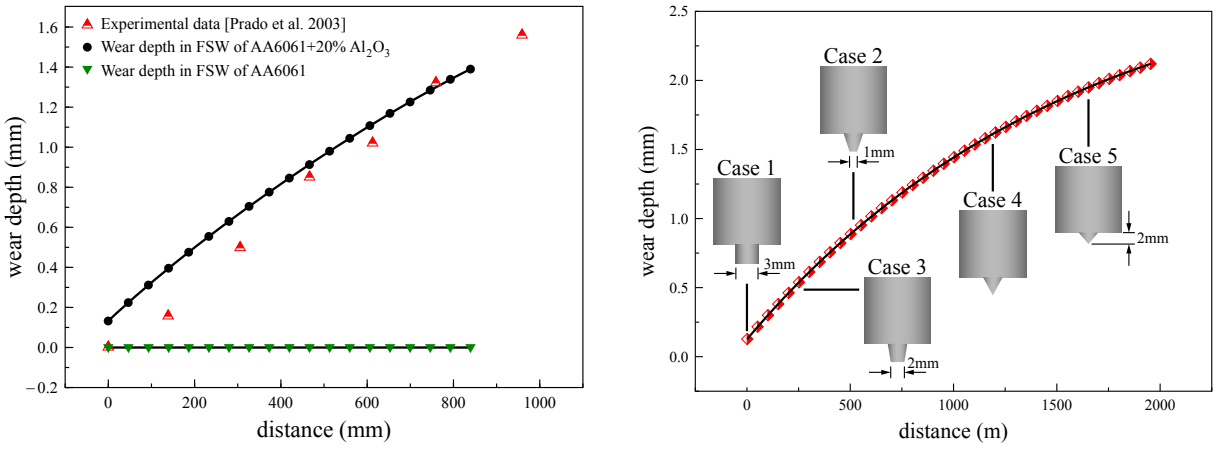

Figure 4. Left: comparison of tool wear with experimental data. Right: tool wear in FSW of AA6061-T6.

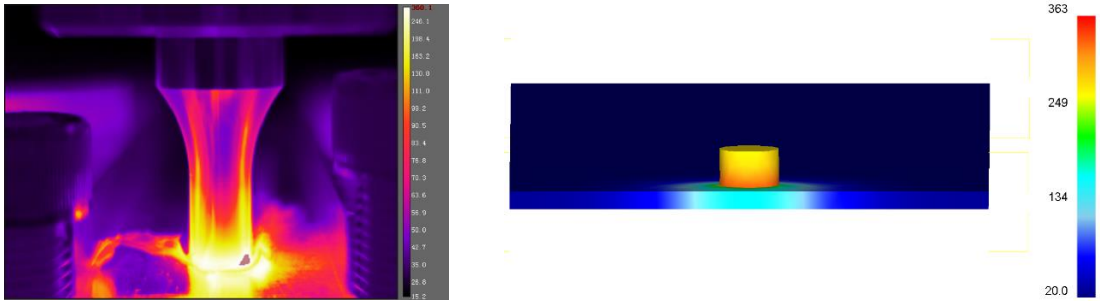

Figure 5. Comparison of predicted and experimental temperature: predicted temperature in Case 2 (left) and temperature image observed by Infrared Radiation Thermometer (right).

This phenomenon is clearly observed in the experiment performed by Sahlot and Arora [2018]. The change in the pin profile due to wear can lead to changes in the temperatures and microstructural evolutions in FSW. Determining how the tool wear affects the temperatures and deformations in the FSW process is key for investigations on the microstructural evolutions in FSW with worn tools. Therefore, four different worn tools were selected for further simulations. Case 1 represents the initial cylindrical tool without wear. Cases 2–4 represent the worn tools with worn distances ranging from 225 m–1425.5 m, as shown in Figure 4 (right).

Figure 5 shows a comparison of the predicted temperature from the adaptive remeshing model and the experimental temperature observed by the infrared radiation thermometer, showing that the results agree well with each other. However, the temperature field under the shoulder cannot be directly observed by the infrared radiation thermometer. Therefore, the maximum welding temperature extracted under the shoulder in the numerical model is usually higher than that observed, as can be seen in Figure 6.

Figure 6 shows the predicted temperature histories in FSW processes with different worn tools. With the increase of the wear depth, the maximum welding temperature decreases. The temperature during

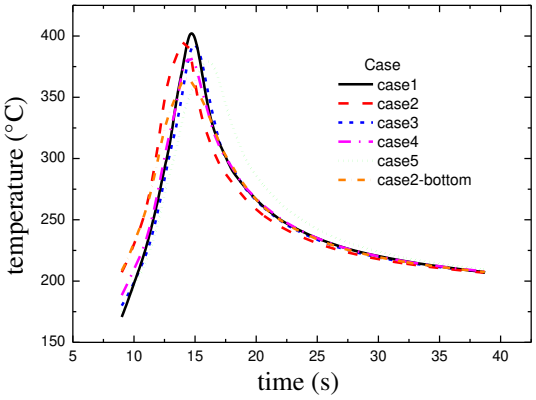

Figure 6. Temperature histories in FSW with different worn tools.

FSW is determined by the frictional and plastic dissipations, as indicated in [Zhang and Zhang 2009], with friction being the main contributor. Compared with Case 1, the pin-plate bottom contact surface decreased by 55.6% in Case 2, 88.9% in Case 3, and becomes zero in Cases 4 and 5. The decrease of the pin-plate bottom contact surface leads to the decrease of the welding temperature with the increase of tool wear.

Additionally, the change in the tool profile due to wear can lead to different grain evolutions in FSW. A Monte Carlo method was used to simulate the nucleation in dynamic recrystallization and the following grain growth. To validate the Monte Carlo method, an experiment was performed using the machine shown in Figure 1. The worn tool in Case 2 was used for the comparison of the numerical and experimental results, as shown in Figure 7. The grain sizes near the top and bottom surfaces are different. Due to the higher temperature near the top surface, the grain size near this area is larger than that near the bottom surface. This observation was also made in the 3D Monte Carlo simulation in the previous work by Zhang and Hu [2018]. The average grain size was 12.1 μm on point 1 and 11 μm on point 2 in the experiment. The predicted values on point 1 and point 2 in the numerical model were 12.7 μm and 11.4 μm, respectively. In addition, the average grain size was 11.5 μm on point 3 and 10.8 μm on point 4 in the experiment. Meanwhile, the predicted values on point 3 and point 4 in the numerical model were 12.3 μm and 10.9 μm, respectively. This shows that the numerical model fitted well with the experimental measurements.

The nine points shown in Figure 8 (left) were selected to calculate the average strain rates in different FSW processes with different worn tools. Figure 8 (right) shows the calculated strain rates in FSW with different worn tools. It indicates that the appropriate tool wear can increase the strain rates in FSW whereas excess tool wear can lead to a decrease of the strain rates. The strain rate is a key factor for determining the nucleation in recrystallization. The increase of the strain rate can lead to an increase of the nucleation rate, and vice versa, according to (7).

The calculated nucleation rate histories in FSW with different worn tools are shown in Figure 9. The point 1.5 mm away from the top surface was selected for comparison. For Case 2, the maximum nucleation rate increased to $8.58 \cdot 10^{12}\,\mathrm{s}^{-1}\,\mathrm{m}^{-3}$ from $7.98 \cdot 10^{12}\,\mathrm{s}^{-1}\,\mathrm{m}^{-3}$ in Case 1. In Cases 3–5, the maximum nucleation rates decreased to $4.42 \cdot 10^{12}\,\mathrm{s}^{-1}\,\mathrm{m}^{-3}$, $3.02 \cdot 10^{12}\,\mathrm{s}^{-1}\,\mathrm{m}^{-3}$, and $2 \cdot 10^{12}\,\mathrm{s}^{-1}\,\mathrm{m}^{-3}$, respectively.

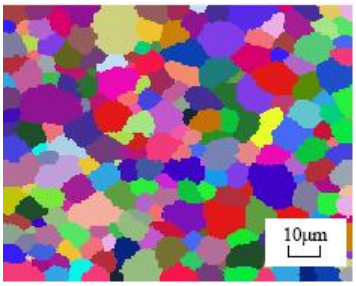

point 1

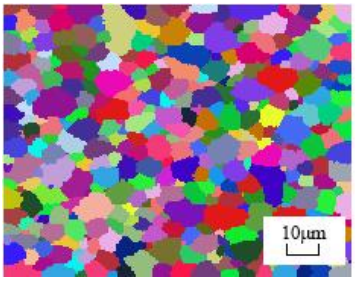

point 2

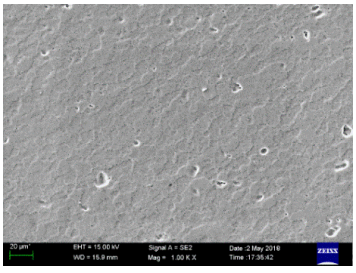

point 1

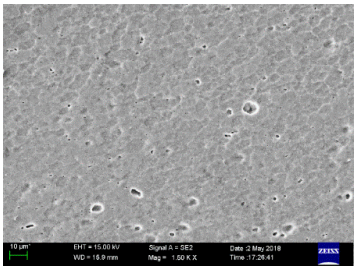

point 2

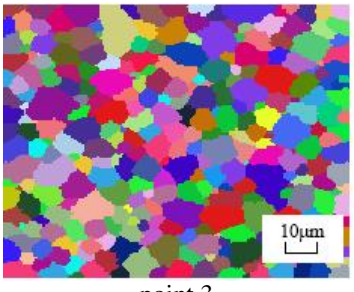

point 3

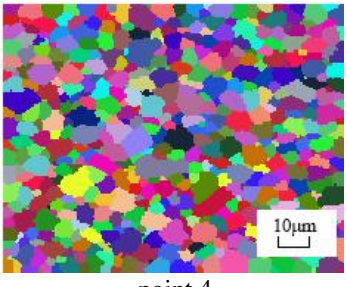

point 4

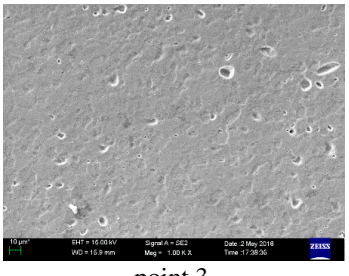

point 3

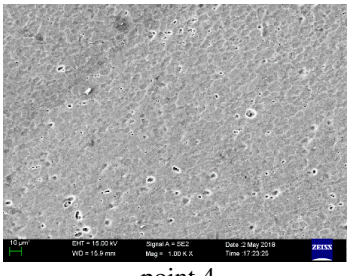

point 4

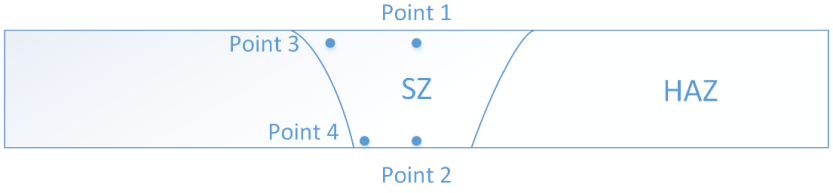

The location of selected point in experiment

Figure 7. Comparison of predicted grains with experiment in Case 2.

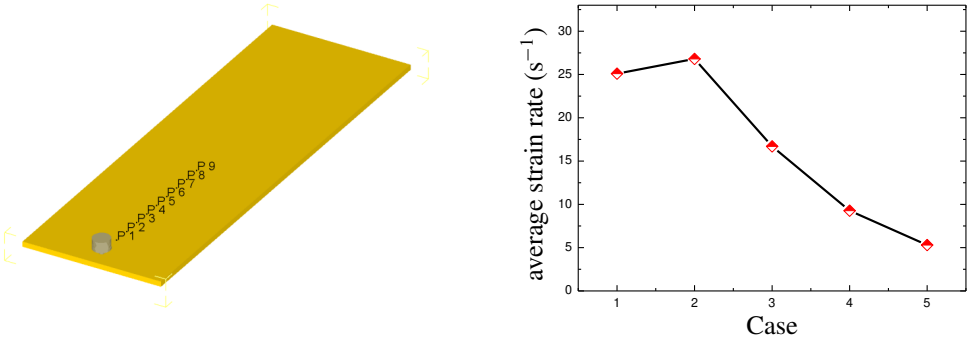

Figure 8. Effect of tool wear on strain rates: nine points selected for computation (left) and calculated strain rates (right).

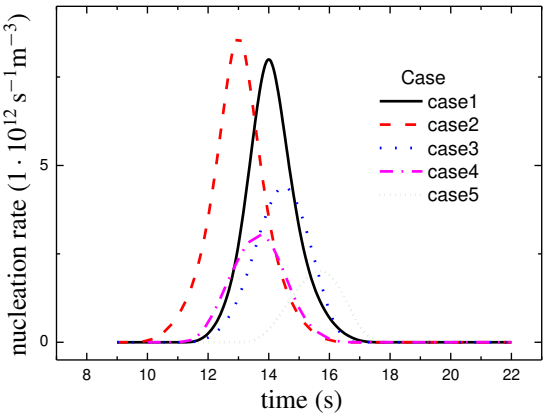

Figure 9. Nucleation rates in different worn tools.

Using the calculated nucleation rates shown in Figure 9, the grain sizes in the FSW with different worn tools could be predicted, as shown in Figure 10. In the FSW with the initial tool without wear (Case 1), the average grain size was 13.2 μm. For Case 2, the average grain size decreased to 12.7 μm. While for Cases 3–5, the average grain sizes increased to 14.1 μm, 15.2 μm, and 16.7 μm, respectively. Appropriate tool wear can lead to smaller grains in the SZ and lead to improvement of the welding quality. However, excess tool wear can lead to the coarsening of the grains in the SZ. This indicates that self-optimization exists in FSW, but the control of the tool wear remains important for the control of the final welding quality in FSW.

The variations of the grain sizes with time in different FSW processes with different worn tools are summarized in Figure 11. The tool wear can obviously affect the grain growth in FSW. The differences between the numerical model and the experiment are 4.96% for point 1, 3.63% for point 2, 6.96% for point 3 and 0.9% for point 4. The error for point 3 is higher than the other points. This is caused by the generation of flash in this region [Kumar et al. 2013]. This can lead to errors on the prediction of strain rates and then affect the predictions of microstructural evolutions. But the comparison shows the proposed models are successful in almost all the regions in the stirring zone. With validation from the experiment, the Monte Carlo method becomes an efficient tool for the design of an appropriate tool pin profile for the optimal welding quality.

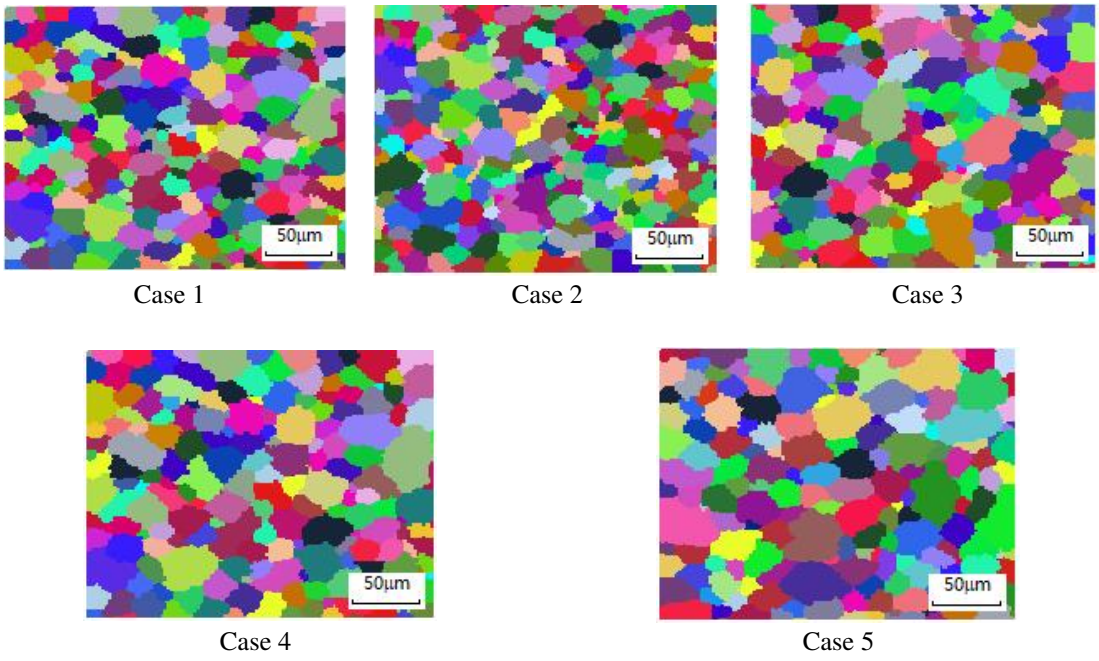

Figure 10. Predicted grain morphologies in FSW with worn tools.

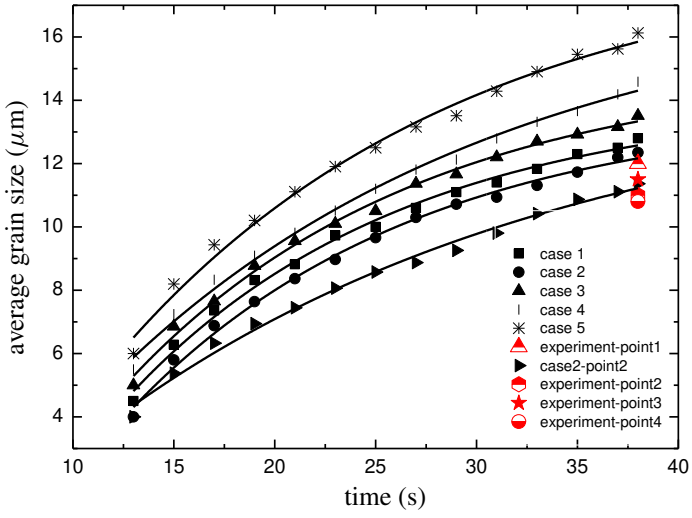

Figure 11. Variations of average grain sizes in FSW with worn tools.

5. Conclusions

(1) Tool wear can lead to a decrease of the wear rate in FSW.

(2) Appropriate tool wear can lead to the formation of smaller equiaxed grains in the SZ. However, excess tool wear can lead to the coarsening of grains in the SZ in FSW.

(3) Strain rate is a key factor for controlling the self-optimization of the tool in FSW.

Acknowledgement

This study was funded by the National Natural Science Foundation of China (No. 11572074).

The authors declare that they have no conflict of interest.

References

[Akbari et al. 2016] M. Akbari, P. Asadi, M. B. Givi, and P. Zolghadr, "A cellular automaton model for microstructural simulation of friction stir welded AZ91 magnesium alloy", *Model. Simul. Mater. Sci. Eng.* **24**:3 (2016), 035012.

[Beygi et al. 2018] R. Beygi, M. Z. Mehrizi, D. Verdera, and A. Loureiro, "Influence of tool geometry on material flow and mechanical properties of friction stir welded Al-Cu bimetals", *J. Mater. Process. Technol.* **255** (2018), 739–748.

[Chen and Nakata 2009] Y. C. Chen and K. Nakata, "Effect of tool geometry on microstructure and mechanical properties of friction stir lap welded magnesium alloy and steel", *Mater. Des.* **30**:9 (2009), 3913–3919.

[De et al. 2014] A. De, H. K. D. H. Bhadeshia, and T. DebRoy, "Friction stir welding of mild steel: tool durability and steel microstructure", *Mater. Sci. Technol.* **30**:9 (2014), 1050–1056.

[Ebrahimpour et al. 2019] A. Ebrahimpour, A. Mostafapour, and K. Samadian, "Finite element and experimental investigation on the effects of temperature, strain and strain rate on microstructure and mechanical properties of FSSWed TRIP steel joints", *Mater. Res. Express* **6**:1 (2019), 016559.

[Grujicic et al. 2015] M. Grujicic, S. Ramaswami, J. S. Snipes, V. Avuthu, R. Galgalikar, and Z. Zhang, "Prediction of the grain-microstructure evolution within a Friction Stir Welding (FSW) joint via the use of the Monte Carlo simulation method", *J. Mater. Eng. Perform.* **24**:9 (2015), 3471–3486.

[He et al. 2017] W. J. He, L. Zheng, R. L. Xin, and Q. Liu, "Microstructure-based modeling of tensile deformation of a friction stir welded AZ31 Mg alloy", *Mater. Sci. Eng. A* **687** (2017), 63–72.

[Kumar et al. 2013] M. Kumar, S. V. Kailas, and R. G. Narayanan, "Influence of external weld flash on the in-plane plane-strain formability of friction stir welded sheets", *J. Strain Anal. Eng. Des.* **48**:6 (2013), 376–385.

[Lee and Jou 2003] R. S. Lee and J. L. Jou, "Application of numerical simulation for wear analysis of warm forging die", *J. Mater. Process. Technol.* **140**:1-3 (2003), 43–48.

[Mastanaiah et al. 2018] P. Mastanaiah, A. Sharma, and G. M. Reddy, "Role of hybrid tool pin profile on enhancing welding speed and mechanical properties of AA2219-T6 friction stir welds", *J. Mater. Process. Technol.* **257** (2018), 257–269.

[Mehta et al. 2011] M. Mehta, A. Arora, A. De, and T. DebRoy, "Tool geometry for friction stir welding — optimum shoulder diameter", *Metall. Mater. Trans. A* **42**:9 (2011), 2716–2722.

[Prado et al. 2001] R. A. Prado, L. E. Murr, D. J. Shindo, and K. F. Soto, "Tool wear in the friction-stir welding of aluminum alloy 6061+20% Al_2O_3: a preliminary study", *Scr. Mater.* **45**:1 (2001), 75–80.

[Prado et al. 2003] R. A. Prado, L. E. Murr, K. F. Soto, and J. C. McClure, "Self-optimization in tool wear for friction-stir welding of Al 6061+20% Al_2O_3 MMC", *Mater. Sci. Eng. A* **349**:1-2 (2003), 156–165.

[Sahlot and Arora 2018] P. Sahlot and A. Arora, "Numerical model for prediction of tool wear and worn-out pin profile during friction stir welding", *Wear* **408-409** (2018), 96–107.

[Sahlot et al. 2018] P. Sahlot, K. Jha, G. K. Dey, and A. Arora, "Wear-induced changes in FSW tool pin profile: effect of process parameters", *Metall. Mater. Trans. A* **49**:6 (2018), 2139–2150.

[Saluja et al. 2012] R. S. Saluja, R. G. Narayanan, and S. Das, "Cellular automata finite element (CAFE) model to predict the forming of friction stir welded blanks", *Comput. Mater. Sci.* **58** (2012), 87–100.

[Shindo et al. 2002] D. J. Shindo, A. R. Rivera, and L. E. Murr, "Shape optimization for tool wear in the friction-stir welding of cast AI359-20% SiC MMC", *J. Mater. Sci.* **37**:23 (2002), 4999–5005.

[Song et al. 2014] K. J. Song, Z. B. Dong, K. Fang, X. H. Zhan, and Y. H. Wei, "Cellular automaton modelling of dynamic recrystallisation microstructure evolution during friction stir welding of titanium alloy", *Mater. Sci. Technol.* **30**:6 (2014), 700–711.

[Suresha et al. 2011] C. N. Suresha, B. M. Rajaprakash, and S. Upadhya, "A study of the effect of tool pin profiles on tensile strength of welded joints produced using friction stir welding process", *Mater. Manuf. Process.* **26**:9 (2011), 1111–1116.

[Valvi et al. 2016] S. R. Valvi, A. Krishnan, S. Das, and N. R. G., "Prediction of microstructural features and forming of friction stir welded sheets using cellular automata finite element (CAFE) approach", *Int. J. Mater. Form.* **9**:1 (2016), 115–129.

[Wan et al. 2016] Z. Y. Wan, Z. Zhang, and X. Zhou, "Finite element modeling of grain growth by point tracking method in friction stir welding of AA6082-T6", *Int. J. Adv. Manuf. Technol.* **90**:9-12 (2016), 3567–3574.

[Wu and Zhang 2017] Q. Wu and Z. Zhang, "Precipitation-induced grain growth simulation of friction-stir-welded AA6082-T6", *J. Mater. Eng. Perform.* **26**:5 (2017), 2179–2189.

[Yang et al. 2018] C. Yang, D. R. Ni, P. Xue, B. L. Xiao, W. Wang, K. S. Wang, and Z. Y. Ma, "A comparative research on bobbin tool and conventional friction stir welding of Al-Mg-Si alloy plates", *Mater. Charact.* **145** (2018), 20–28.

[Zhang and Hu 2018] Z. Zhang and C. P. Hu, "3D Monte Carlo simulation of grain growth in friction stir welding", *J. Mech. Sci. Technol.* **32**:3 (2018), 1287–1296.

[Zhang and Wan 2012] Z. Zhang and Z. Y. Wan, "Predictions of tool forces in friction stir welding of AZ91 magnesium alloy", *Sci. Technol. Weld. Join.* **17**:6 (2012), 495–500.

[Zhang and Wu 2015] Z. Zhang and Q. Wu, "Numerical studies of tool diameter on strain rates, temperature rises and grain sizes in friction stir welding", *J. Mech. Sci. Technol.* **29**:10 (2015), 4121–4128.

[Zhang and Zhang 2007] Z. Zhang and H. W. Zhang, "The simulation of residual stresses in friction stir welds", *J. Mech. Mater. Struct.* **2**:5 (2007), 951–964.

[Zhang and Zhang 2009] Z. Zhang and H. W. Zhang, "Numerical studies on controlling of process parameters in friction stir welding", *J. Mater. Process. Technol.* **209**:1 (2009), 241–270.

[Zhang et al. 2009] Z. Zhang, Y. L. Liu, and J. T. Chen, "Effect of shoulder size on the temperature rise and the material deformation in friction stir welding", *Int. J. Adv. Manuf. Technol.* **45**:9 (2009), 889–895.

[Zhang et al. 2014] Z. Zhang, Q. Wu, and H.-W. Zhang, "Numerical studies of effect of tool sizes and pin shapes on friction stir welding of AA2024-T3 alloy", *Trans. Nonferr. Met. Soc. China* **24**:10 (2014), 3293–3301.

[Zhang et al. 2016] Z. Zhang, Q. Wu, M. Grujicic, and Z. Y. Wan, "Monte Carlo simulation of grain growth and welding zones in friction stir welding of AA6082-T6", *J. Mater. Sci.* **51**:4 (2016), 1882–1895.

[Zhang et al. 2017] Z. Zhang, Z. Y. Wan, L.-E. Lindgren, Z. J. Tan, and X. Zhou, "The simulation of precipitation evolutions and mechanical properties in friction stir welding with post-weld heat treatments", *J. Mater. Eng. Perform.* **26**:12 (2017), 5731–5740.

Received 2 Mar 2019. Revised 30 Jul 2019. Accepted 15 Aug 2019.

ZHAO ZHANG: zhangz@dlut.edu.cn
Department of Engineering Mechanics, Dalian University of Technology, No. 2 Linggong Road, Dalian, 116024, China

ZHIJUN TAN: 742046605@qq.com
Department of Engineering Mechanics, Dalian University of Technology, No. 2 Linggong Road, Dalian, 116024, China

JOURNAL OF MECHANICS OF MATERIALS AND STRUCTURES

msp.org/jomms

Founded by Charles R. Steele and Marie-Louise Steele

Cover photo: Mando Gomez, www.mandolux.com

See msp.org/jomms for submission guidelines.

JoMMS (ISSN 1559-3959) at Mathematical Sciences Publishers, 798 Evans Hall #6840, c/o University of California, Berkeley, CA 94720-3840, is published in 10 issues a year. The subscription price for 2019 is US $635/year for the electronic version, and $795/year (+$60, if shipping outside the US) for print and electronic. Subscriptions, requests for back issues, and changes of address should be sent to MSP.

JoMMS peer-review and production is managed by EditFLOW® from Mathematical Sciences Publishers.

PUBLISHED BY

mathematical sciences publishers

nonprofit scientific publishing

http://msp.org/

Journal of Mechanics of Materials and Structures

Volume 14, No. 4 July 2019

1559-3959(2019)14:4;1-U